N. Winzer[1], G. Song[1], A. Atrens[1], W. Dietzel[2], K.U. Kainer[2]
[1]Materials Engineering, The University of Queensland, Brisbane, Australia
[2]GKSS-Forschungszentrum Geesthacht GmbH, Germany

STRESS CORROSION CRACKING OF MAGNESIUM

ABSTRACT

The increased use of Mg-alloys for stressed automotive components has created a demand for a better mechanistic understanding of the environmental and mechanical influences contributing to Transgranular Stress Corrosion Cracking (TGSCC). TGSCC is the inherent mode of failure for Mg alloys exposed to aqueous environments below their yield stress. It is generally accepted that the predominant mechanism(s) for TGSCC is a type of Hydrogen Assisted Cracking (HAC); however, the specific nature of this mechanism(s) is equivocal. The most commonly proposed mechanism is Delayed Hydride Cracking (DHC). This work investigates its tenability by comparing experimental measurements of the stress corrosion crack velocity, V_c, with predictions based on a numerical model for DHC. The measured velocity was in the range of $7x10^{-10}$ m/s to $5x10^{-9}$ m/s. The initial prediction of the DHC model is ~$5x10^{-7}$ m/s. An investigation into the sensitivity of the model to input parameters is currently underway.

Key words: *Transgranular stress corrosion cracking, hydrogen assisted cracking, delayed hydride cracking, fractography, stress assisted diffusion, magnesium, hydrogen*

BACKGROUND AND INTRODUCTION

Our recent critical review [1] indicated that many Mg alloys are susceptible to SCC at stresses as low as 50% of σ_Y for many common service environments. It is generally accepted that TGSCC is the inherent mode of fracture for Mg alloys at loads below σ_Y; however, there is a general lack of understanding regarding the mechanism(s) responsible for TGSCC. Previous workers generally agreed that TGSCC of Mg alloys somehow involves Hydrogen Embrittlement (HE) and various HE mechanisms have been proposed, namely H-Enhanced Decohesion (HEDE), H-Enhanced Localized Plasticity (HELP), Adsorption Induced Dislocation Emission (AIDE) and Delayed Hydride Cracking (DHC). DHC is the most strongly supported of these [2, 3, 4, 5]. DHC involves repeated stages of stress-assisted diffusion of H toward the area ahead of the crack tip leading to hydride formation and fracture. More detail on these mechanisms is given by Lynch [6].

Considering the wide range of crack velocities reported by previous workers, it is possible that more than one mechanism is prevalent and that the predominant mechanism is related to crack velocity. Lynch and Trevena [7] proposed that the inherent mechanism for HE in pure Mg for crack velocities >10^{-8} m/s is AIDE, which involves adsorption of H atoms at the crack tip, since insufficient time would be

available for H to diffuse ahead of the crack; however, they proposed that a mechanism involving diffusion (such as HEDE or DHC) may predominate at lower crack velocities. It is also possible that the relationship between crack velocity and HE mechanism is due to variations in the crack tip geometry and therefore intra-crack H transport with applied stress, as proposed by Makar et al [5].

Numerical models may provide insight into the mechanism(s) for SCC of Mg alloys by predicting the crack velocity, V_C; however, the usefulness of numerical models is limited by the availability of material properties. For example, discrepancies regarding the predominant mechanism for TGSCC may be partly attributed to the use of speculative values for the diffusion coefficient for H dissolved in Mg. The coefficient is difficult to measure by classical permeation studies due to the presence of rapidly forming and relatively impermeable layers at the Mg surface. Consequently, there is no data for the H diffusion coefficient for Mg alloys near room temperature, although values between 10^{-9} m^2/s and 10^{-12} m^2/s have been estimated by extrapolating data from elevated temperatures [8].

The work described herein is part of a research program aimed at developing a mechanistic understanding of the influence of environmental parameters on SCC susceptibility of Mg alloys. Work so far has focused on identifying mechanical and environmental conditions causing TGSCC and determining typical values for V_c. This paper introduces a numerical model for predicting V_c and describes our initial attempt at correlating theoretical and measured values for V_c in order to identify the mechanism.

CHARACTERISATION OF TGSCC

Experimental Method

SCC tests were performed using high purity AZ91 (> 90.11wt%Mg, 8.99wt%Al, 0.78wt%Zn, 0.21wt%Mn). Cylindrical tensile specimens with 5 mm diameter waisted gauge were machined from as-cast ingots. The gauge surface was polished with 600 grit emery paper and the specimens were degreased in ethanol before use. The test environments were double-distilled water and laboratory air. All tests were conducted at open-circuit conditions.

Mechanical loads were applied under linearly increasing stress test (LIST) or strain rate test (SSRT) conditions. A comparison of these two methods was given by Winzer et al [9]. In the LIST apparatus (Figure 1) the specimen is attached to one end of a lever arm. To the opposite end of the arm a known mass is attached such that the tensile load applied to the specimen increases linearly as the distance between the fulcrum and the mass is increased by means of a screw thread and synchronous motor. The SSRT apparatus (Figure 2) maintains a constant strain rate by means of an open-loop control system; the average specimen elongation is measured by two high-resolution LVDTs in parallel with the specimen whilst a geared synchronous motor increases the elongation and thus the load accordingly.

SCC susceptibility was characterised according to the threshold stress, which was determined using the DC potential drop (DCPD) method [10, 11, 12, 13, 14, 15]. The DCPD method involves applying a low constant current to the specimen and measuring the change in specimen resistance as the cross-section is reduced, primarily by crack

propagation, according to the relationship $\Delta R=\rho l/\Delta A$, where ΔA is the change in cross-sectional area, ρ is the resistivity and l is the length of the specimen. A pulsed and reversing current was used to minimise thermoelectric offset voltages due to coupling of dissimilar metals in a variable-temperature environment. Variations in the resistivity of the specimen due to temperature were accounted for by using a reference specimen.

V_c was calculated for both LIST and SSRT conditions according to $V_c = a/t$ where a is the length of the stress corrosion crack at the end of the test as estimated from the fracture surface and t is the time for stress corrosion crack growth from crack initiation (identified using the DCPD method) to the end of the test.

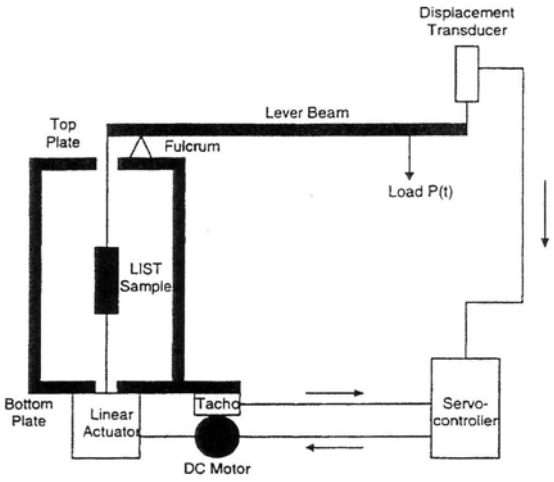

Fig. 1. Schematic illustration of the LIST apparatus

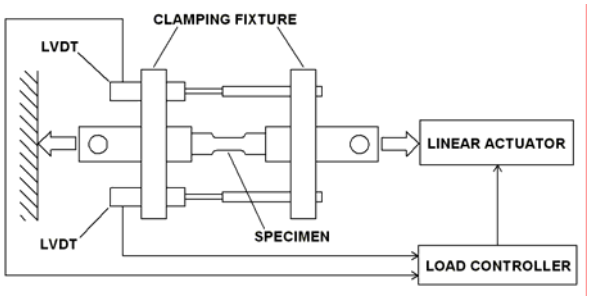

Fig. 2. Schematic illustration of the SSRT apparatus

Experimental Results

Figures 3 and 4 show the stress-strain behaviour and DCPD measurements respectively for SSRT tests in distilled water and in air. There was a considerable reduction in the UTS relative to air for all of the samples exposed to distilled water. Moreover, for the specimens exposed to distilled water the threshold stress and UTS decreased with decreasing strain rate. The threshold stress was interpreted as corresponding to the point where the DCPD curve became non-linear (Figure 4). The threshold stresses at $3x10^{-8}$ s^{-1}, 10^{-7} s^{-1} and $3x10^{-7}$ s^{-1} were approximately 55 MPa, 65 MPa and 75 MPa respectively. The periods of time between the DCPD curve becoming non-linear and cessation of the test (or time corresponding to SCC) for these strain rates were 264 h, 80 h and 42 h respectively.

Fracture surfaces for specimens tested under SSRT conditions in distilled water at $3x10^{-8}$ s^{-1}, 10^{-7} s^{-1} and $3x10^{-7}$ s^{-1} were partly comprised of relatively flat regions containing predominantly coarse stepped markings typically 5 μm apart as shown in Figures 5A and 5B. The parallel edges featured considerable amounts of jogging. Secondary cracks were also evident. The regions were discrete in size and invariably found at the surface of the specimen as shown in Figure 5C. The maximum depth of the regions in each case was 500 μm to 1000 μm. The remaining fracture surface was generally comprised of broken, jagged regions with some randomly interspersed dimpled regions for the specimen fractured at $3x10^{-7}$ s^{-1} (Figure 5D).

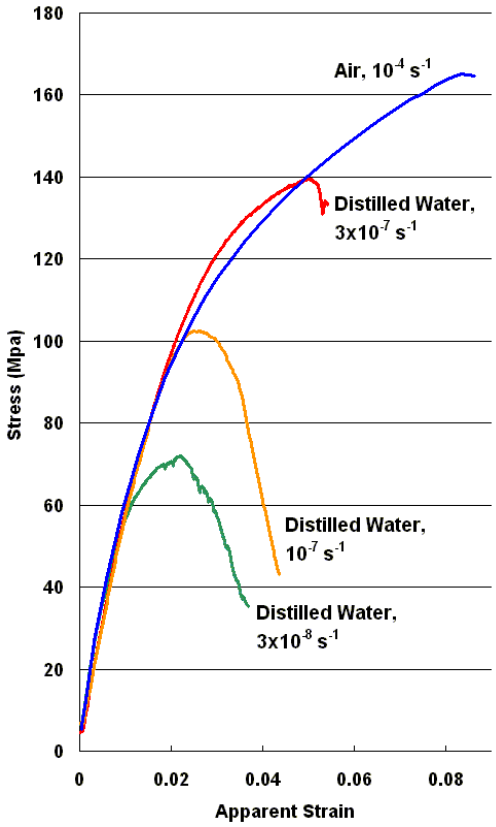

Fig. 3. Stress-strain curves for AZ91 in distilled water and air

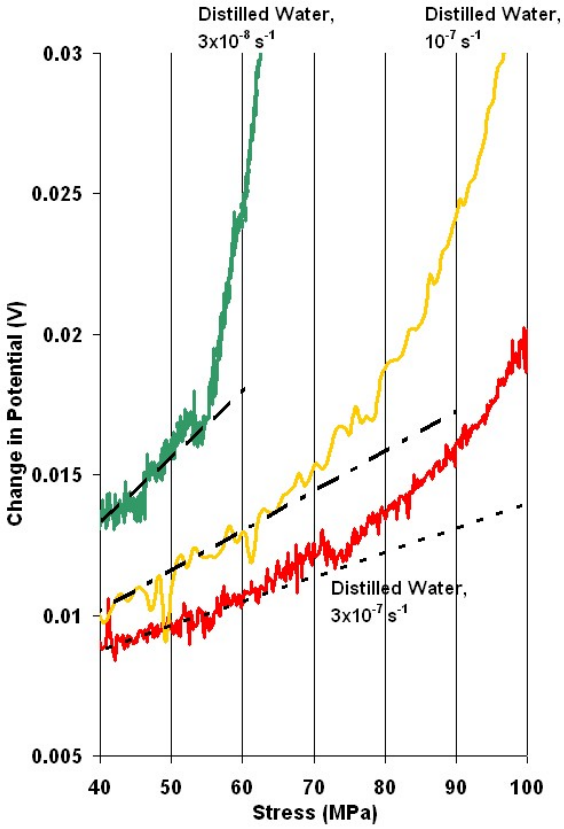

Fig. 4. DCPD results for AZ91 in distilled water and air

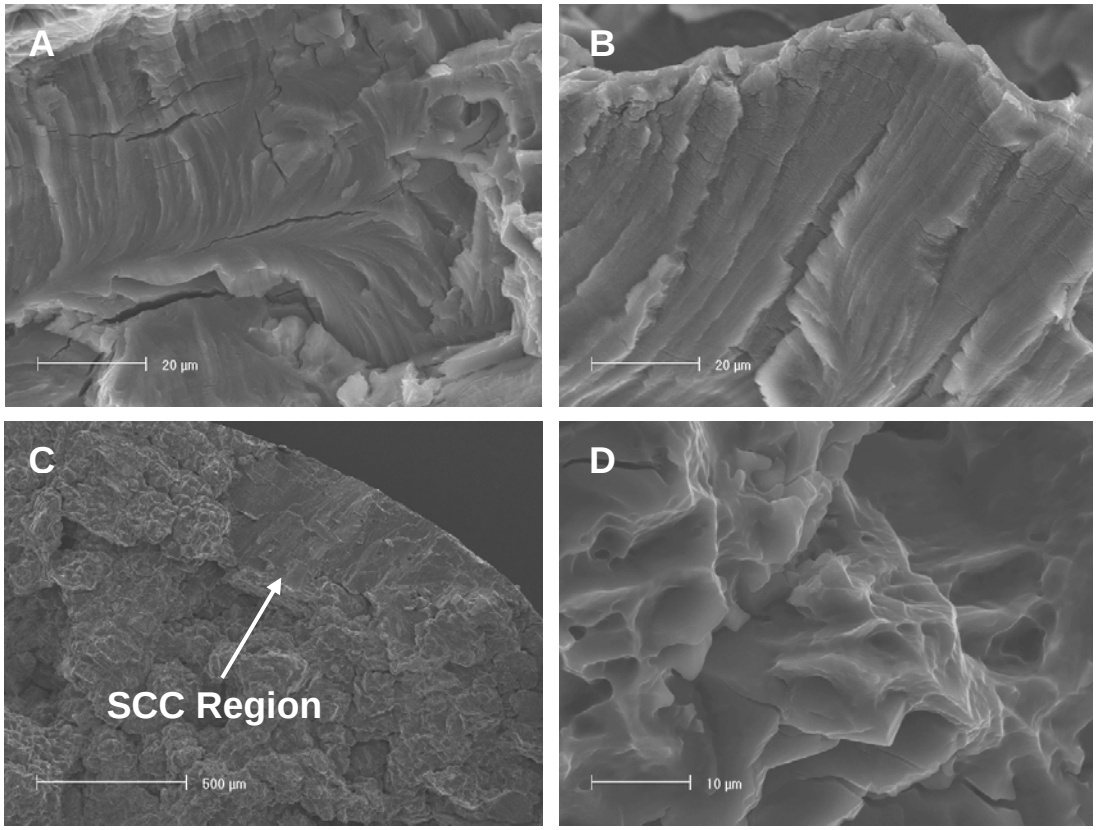

Fig. 5. SEM micrographs for specimens fractured in distilled water at 10^{-7} s^{-1} (A), $3x10^{-8}$ s^{-1} (B and C) and $3x10^{-7}$ s^{-1} (D)

DHC MODEL

A finite element program was developed in MATLAB to simulate H diffusion due to stress and concentration gradients and hydride precipitation [16]. The cross section of the crack was discretised using a mesh of 1200 uniform linear triangular elements with the crack surface as part of the lower boundary. A small uniform concentration was applied to the mesh at $t = 0$ and maintained at the crack surface for all t. Flux was enabled at the crack surface and all other boundaries except for that ahead of the crack tip. The iterative procedure was based on the following matrix equations for H diffusion and hydride precipitation in Zr alloys by Sofronis et al [17, 18] and Varias et al [19, 20, 21]:

$$\left[\frac{1}{\Delta t}[M]_t + [K_1]\right]\{C\}_{t+\Delta t} = \frac{1}{\Delta t}[M]_t\{C\}_t + \{F\}_t - [K_2]\{C\}_t \quad (1)$$

$$[M] = \int_V [A]^T [A] dV \quad (2)$$

$$[K_1] = \int_V [B]^T D[B] dV \quad (3)$$

$$[K_2] = \int_V [B]^T \frac{D\bar{V}_H}{3kT}[B]\{\sigma_{kk}\}[A] dV \quad (4)$$

$$\{F\} = -\int_S [A]^T \mathbf{J} dS \quad (5)$$

where $\{C\}$ is the nodal concentration vector, $\{F\}$ contains the flux at the boundary, $\{\sigma_{kk}\}$ is a time-independent vector containing nodal values for the K_1-mode hydrostatic stress field near the crack tip, $[A]$ and $[B]$ are the standard time-independent interpolation matrices for transient diffusion problems, **J** is the component of the flux normal to the bounding surface S (calculated according to Fick's Second Law), $[M]$ is the so-called concentration matrix and $[K_1]$ and $[K_2]$ are the so-called diffusivity matrices corresponding to concentration and stress directed diffusion respectively.

The model differed from that described by Sofronis et al [17, 18] in that it neglected the influence of hydride formation on the stress field. Hydride precipitation is accompanied by deformation of the lattice due to the dissimilar atomic volumes of the composing materials. The deformation is coupled with the precipitation process in that the resulting disturbance in the stress field decreases the force driving H diffusion. However, by maintaining a constant stress field it is unnecessary to calculate changes in the stress field for each iteration, considerably reducing the computation intensity.

For each iteration the hydride volume fraction, f, was calculate at each node by linearly interpolating between $f = 0$ at the solvus concentration and $f = 1$ at the molar concentration of H in pure hydride (0.33 in the case of MgH_2). In the absence of other data a solvus concentration of 2 at. % as reported by Krozer and Kasemo [22] was used.

Approximation of V_c requires some awareness of the hydride geometry required for fracture. Mg SCC fracture surfaces are typified by coarse, parallel markings as shown in Figure 4. These may correspond to preferential cleavage planes [2]. Previous workers have also reported fine parallel markings approximately 0.1 - 0.8 μm within these cleavage planes [3, 4, 26]. A V_c of 5×10^{-7} m/s was calculated from $V_c = l/t$, where l

was 0.8 μm and *t* was the time required for the $f = 1$ hydride front to reach 0.8 μm ahead of the crack tip, as shown in Figure 6. This calculation assumed $D = 10^{-9}$ m^2/s and $K_1 = 15.9$ MPa/m$^{1/2}$ and that the stress corrosion crack propagates through the region where $f = 1$ only.

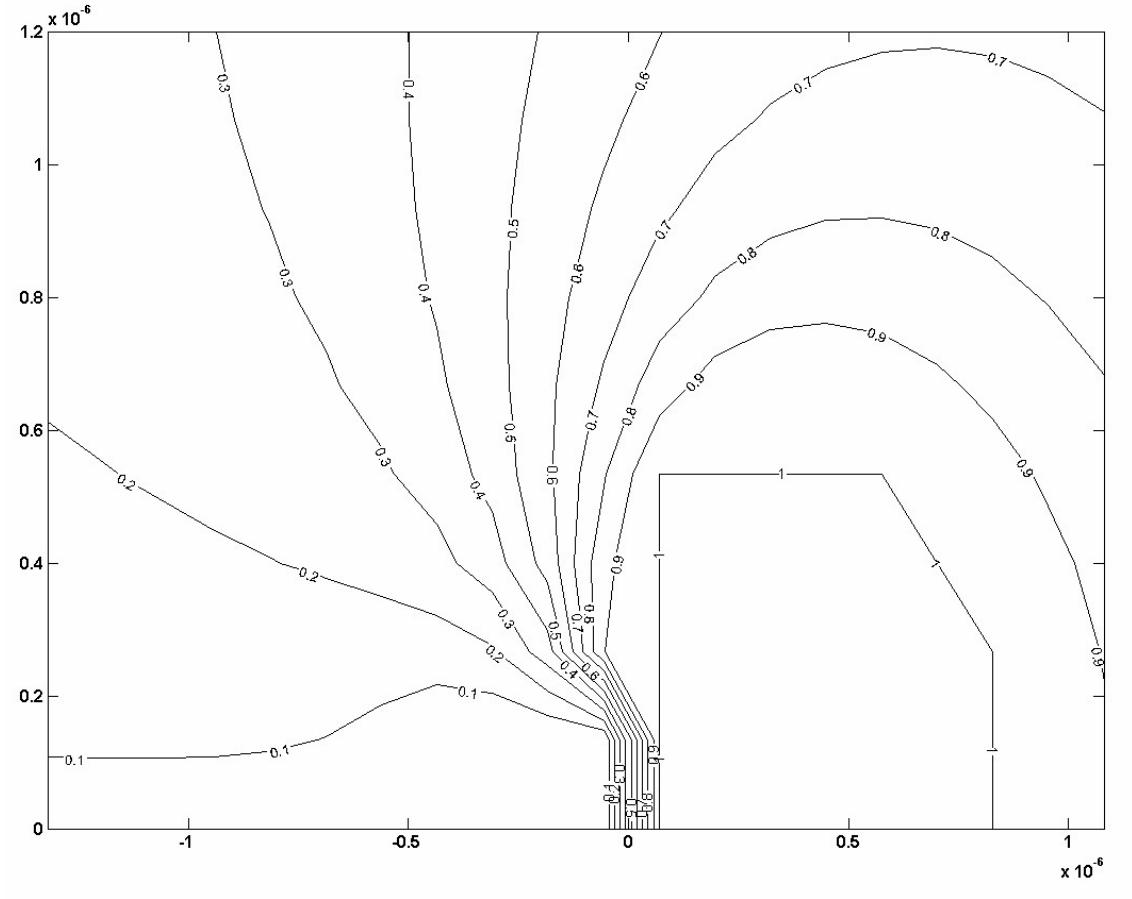

Fig. 6. Hydride volume fraction ahead of the crack tip after ~1.6sec

DISCUSSION

Figures 3 and 4 show for AZ91 in distilled water at $3x10^{-8}$ s^{-1} to $3x10^{-7}$ s^{-1} there was a reduction in UTS relative to air that is indicative of SCC. Ebtehaj et al [23] and Wearmouth et al [24] found that for Mg-Al alloys in solutions containing approximately equal concentrations of chloride and chromate ions maximum susceptibility occurred at a discrete range of intermediate strain rates; at low strain rates repassivation retarded H-ingress at mechanical film rupture sites whereas at high strain rates ductile tearing predominated. In the present case, there was no evidence of ductile tearing on the fracture surface corresponding to steady-state crack propagation for SSRT tests between $3x10^{-8}$ s^{-1} and $3x10^{-7}$ s^{-1}. The fact that the UTS and threshold stress decreased with decreasing strain rate suggests that SCC susceptibility was dependent on the balance between mechanical film rupture and repassivation between $3x10^{-8}$ s^{-1} and $3x10^{-7}$ s^{-1}. It may be important to note that this study included only a limited range of strain rates; a

distinct minimum threshold stress or UTS may be identified if the range of strain rates were extended.

The coarse, parallel markings observed for tests in distilled water and 5 g/L NaCl solution were consistent with those observed by Stampella et al [25] for pure Mg anodically polarized in Na_2SO_4 solution, Meletis and Hochman [2] for pure Mg in NaCl-K_2CrO_4 solution and Chakrapani and Pugh [26] and Wearmouth et al [24] for Mg-7.5Al in NaCl-K_2CrO_4 solutions. That these regions were located invariably at surfaces suggests that they correspond to SCC initiation sites. It follows that the periods of time between the DCPD curve becoming non-linear and cessation of the test correspond to SCC propagation. Thus, the maximum dimensions for the areas containing predominantly coarse, parallel markings give experimental values for V_c of $7x10^{-10}$ m/s to $5x10^{-9}$ m/s. These values are considerably lower than the value obtained using the numerical model, indicating the DHC is theoretically possible.

Table 1 summarises measured values for V_c from this work and Table 2 summarises measured V_c values reported by previous workers. The values measured in this work correspond to the lower range of values reported previously, most of which were for very different environments. The present values correspond well to those reported by Spiedel [27] for ZK50A-T6 in distilled water.

Table 1. *Measured stress corrosion crack velocities for AZ91 in distilled water*

Load Condition	**Stress/Strain rate**	***a* (μm)**	***t* (h)**	**V_c (m/s)**
LIST	$7x10^{-3}$ MPa/s	~50	3	$5x10^{-9}$
SSRT	$3x10^{-8}$ s^{-1}	~700	264	$7x10^{-10}$
SSRT	$1x10^{-7}$ s^{-1}	~700	80	$2x10^{-9}$
SSRT	$3x10^{-7}$ s^{-1}	~700	42	$5x10^{-9}$

Table 2. *Measured stress corrosion crack velocities by previous workers for pure Mg and alloys*

Material	**Environment**	**Load Conditions**	**Crack Velocity (m/s)**	**Source**
Mg-7.5Al	NaCl+K_2CrO_4	-	$2.5x10^{-5}$	4
Mg-7.6Al	NaCl+K_2CrO_4	Constant load	$4.2x10^{-5}$-$5.8x10^{-6}$	29
Mg-7Al	NaCl+K_2CrO_4	SSRT	$2 x10^{-6}$-$5x10^{-6}$	24
ZK50A-T5	Distilled H_20	Constant load	$3x10^{-9}$-$8x10^{-9}$	27
ZK50A-T5	1.4m Na_2SO_4	Constant load	$6x10^{-4}$	27
ZK50A-T5	5m NaBr	Constant load	10^{-5}	27
Mg-7.6Al	NaCl+K_2CrO_4	Constant load	10^{-5}	28
Mg-8.8Al	NaCl+K_2CrO_4	SSRT	10^{-7}-$8x10^{-6}$	23
Mg-8.8Al	NaCl+K_2CrO_4	Constant load	$2x10^{-6}$-$3x10^{-5}$	23
Mg-8.8Al	NaCl+K_2CrO_4	Constant strain	$8x10^{-7}$-$2x10^{-5}$	23
RSP Mg-1Al	NaCl+K_2CrO_4	SSRT	$2x10^{-7}$-10^{-5}	5
RSP Mg-9Al	NaCl+K_2CrO_4	SSRT	$8x10^{-8}$-$3x10^{-6}$	5
Pure Mg	NaCl+K_2CrO_4	Const deflection rate	10^{-8}-$5x10^{-2}$	7

Differences in measured values are not remarkable considering that Ebtehaj et al [23] and Makar et al [4] showed that a broad range of crack velocities ($8x10^{-8}$-$2x10^{-5}$m/s) can be achieved by varying the environmental composition and applied stress or

stress intensity. The report by Lynch and Trevena [7] of crack velocities as high as $5x10^{-2}$m/s for pure Mg is anomalous; this was produced by cantilever bend tests at extreme deflection rates although SCC-like fracture surface topography (parallel steps or facets) was observed. It should be noted that these workers used a wide range of techniques to measure V_c. Bursle and Pugh [4] calculated V_c from measured distances between consecutive parallel steps and the time intervals between corresponding acoustic emissions. Pugh et al [29] and Speidel et al [27] measured V_c directly using travelling microscopes. Wearmouth et al [24] measured the crack length by stopping the test at various time intervals. Makar et al [4] divided the length of fracture surface corresponding to SCC by the test duration. The correlation with these workers may improve if similar techniques are used.

SUMMARY

A numerical model for DHC has been introduced. The model has been used to predict stress corrosion crack velocities in Mg alloys. The predicted values were considerably higher than measured values but similar to those reported by previous workers for similar environments. The results of the DHC model are sensitive to various material parameters (such as the diffusivity of H in Mg) that remain unknown. An investigation of the sensitivity of the model to input parameters is currently underway.

ACKNOWLEDGEMENTS

The authors wish to thank the GM Technical Centre at Warren MI, the Australian Research Council (ARC), the Australian Research Network for Advanced Materials (ARNAM) and GKSS-Forschungszentrum Geesthacht GmbH.

REFERENCES

1 Winzer N., Atrens A., Song G., Ghali E., Dietzel W., Kainer K.U., Hort N., Blawert C.: A Critical Review of the Stress Corrosion Cracking (SCC) of Magnesium Alloys, Adv. Eng. Mater., 7, No. 8, 2005, pp. 659-693.

2 Meletis E.I., Hochman R.F.: Crystallography of Stress Corrosion Cracking in Pure Magnesium, Corrosion, 40, 1984, pp. 39-45.

3 Chakrapani D.G., Pugh E.N.: Hydrogen Embrittlement in a Mg-Al Alloy, Met. Trans., 7A, 1976, pp. 173-178.

4 Bursle A.J., Pugh E.N.: On the Mechanism of Transgranular Stress-Corrosion Cracking, Mechanisms of Environment Sensitive Cracking of Materials, Swann P.R., Ford F.P., Westwood A.R.C. [ed.], Materials Society, London, 1977, pp. 471-481.

5 Makar G.L., Kruger J., Sieradzki K.: Stress Corrosion Cracking of Rapidly Solidified Magnesium-Aluminium Alloys, Corros. Sci., 34, No. 8, 1993, pp. 1311-1342.

6 Lynch S.P.: Mechanisms of Hydrogen Assisted Cracking - A Review, Hydrogen Effects on Material Behaviour and Corrosion Deformation Interactions, Moody N.R., Thompson A.W., Ricker R.E., Was G.W., Jones R.H. [ed.], TMS, 2003. pp. 449-466.

7 Lynch S.P, Trevena S.: Stress Corrosion Cracking and Liquid Metal Embrittlement in Pure Magnesium, Corrosion, 44, 1988, pp. 113-124.

8 Atrens A., Winzer N., Song G., Dietzel W., Blawert C.: Stress Corrosion Cracking and Hydrogen Diffusion in Magnesium, Adv. Eng. Mater., 8, 2006, pp. 749-751.

9 Winzer N., Atrens A., Song G., Dietzel W., Blawert C., Kainer K.U.: Evaluation of Mg SCC Using LIST and SSRT, Proceedings of the 7th International Conference on Magnesium Alloys and Their Applications, DGM, Germany, pp. 715-720.

10 Atrens A., Brosnan C.C., Ramamurthy S., Oehlert A., Smith I.O.: Linearly increasing stress test (LIST) for SCC research, Meas. Sci. Technol., 4, 1993, pp. 1281-1292.

11 Oehlert A., Atrens A.: Stress corrosion crack propagation in AerMet 100, J Mater. Sci., 33, 1998, pp. 775-781.

12 Oehlert A., Atrens A.: Environmental assisted fracture for 4340 steel in water and air of various humidities, J Mater. Sci., 32, 1997, pp. 6519-6523.

13 Oehlert A., Atrens A.: The initiation and propagation of stress corrosion cracking in AISI 4340 and 3.5 Ni-Cr-Mo-V rotor steel in constant load tests, Corros. Sci., 38, 1996, pp. 1159-1170

14 Oehlert A., Atrens A.: Room temperature creep of high strength steels, Acta Metall. Mater., 42, 1994, pp. 1493-1508.

15 Dietzel W., Schwalbe K.H.: Monitoring Stable Crack Growth Using a Combined A.C./D.C. Potential Drop Technique, Z. Materialprüfung, 28, No 11, 1986, pp. 368-372.

16 Winzer N., Atrens A., Song G., Dietzel W., Kainer K.U.: Numerical Modelling of TGSCC in Mg Alloys, submitted for publication

17 Lufrano J., Sofronis P., Birnbaum H.K.: Modelling of Hydrogen Transport of Elastically Accommodated Hydride Formation Near a Crack Tip, J. Mech. Phys. Solids, 44, No 2, 1996, pp. 179-205.

18 Sofronis P., McMeeking R.M.: Numerical Analysis of Hydrogen Transport Near a Blunting Crack Tip, J. Mech. Phys. Solids, 37, No 3, 1989, pp. 317-350.

19 Varias A.G., Massih A.R.: Hydride-Induced Embrittlement and Fracture in Metals – Effect of Stress and Temperature Distribution, J. Mech. Phys. Solids, 50, 2002, pp. 1469-1510.

20 Varias A.G., Feng J.L.: Simulation of Hydride Induced Steady-State Crack Growth in Metals – Part I: Growth Near Hydrogen Chemical Equilibrium, Computational Mechanics, 34, 2004, pp. 339-356.

21 Varias A.G., Feng J.L.: Simulation of Hydride Induced Steady-State Crack Growth in Metals – Part II: General Near Tip Field, Computational Mechanics, 34, 2004, pp. 357-376.

22 Krozer A., Kasemo B.: Equilibrium Hydrogen Uptake and Associated Kinetics for the Mg-H2 System at Low Pressures, J. Phys.: Condens. Matter l, 1989, pp. 1533-1538.

23 Ebtehaj K., Hardie D.: Parkins R.N.: The Influence of Chloride-Chromate Solution Composition on the Stress Corrosion Cracking of a Mg-Al Alloy, Corros. Sci., 28, 1993, pp. 811-829.

24 Wearmouth W.R., Dean G.P., Parkins R.N.: Role of Stress in the Stress Corrosion Cracking of a Mg-Al Alloy, Corrosion, 29, No 6, 1979, pp. 251-258.

25 Stampella R.S., Proctor R.P.M., Ashworth V.: Environmentally Induced Cracking of Magnesium, Corros. Sci., 24, No 4, 1984, pp. 325-341.

26 Chakrapani D.G., Pugh E.N.: On the Fractography of Transgranular Stress Corrosion Failures in a Mg-Al Alloy, Corrosion, 31, 1975, pp. 247-252.

27 Speidel M.O., Blackburn M.J., Beck T.R., Feeney J.A.: Corrosion Fatigue and Stress Corrosion Crack Growth in High Strength Aluminium Alloys, Magnesium Alloys and Titanium Alloys Exposed to Aqueous Solutions, Corrosion Fatigue: Chemistry, Mechanics and Microstructure, NACE-2, 1972, pp. 324-345.

28 Chakrapani D.G., Pugh E.N.: The Transgranular SCC of a Mg-Al Alloy: Crystalographic, Fractographic and Acoustic-Emission Studies, Met. Trans., 6A, 1975, pp. 1155-1163.

29 Pugh E.H., Green J.A.S., Slattery P.W.: On the Propagation of Stress-Corrosion Cracks in a Magnesium-Aluminium Alloy, Fracture 1969: The Proceedings of the Second International Conference on Fracture, Pratt P.L. [ed.], Chapman and Hall Ltd, London, 1969, p. 387.